POLITECNICO DI TORINO
Repository ISTITUZIONALE

Adsorption model for biogas purification: A design tool for solid oxide fuel cells applications

Original
Adsorption model for biogas purification: A design tool for solid oxide fuel cells applications / Rozzi, E., Gandiglio, M., Lanzini, A., Santarelli, M.. - In: JOURNAL OF CLEANER PRODUCTION. - ISSN 1879-1786. - ELETTRONICO. - 503:145382(2025), pp. 1-14. [10.1016/j.jclepro.2025.145382]

Availability:
This version is available at: 11583/2998801 since: 2025-04-03T10:54:10Z

Publisher:
Elsevier

Published
DOI:10.1016/j.jclepro.2025.145382

Terms of use:

This article is made available under terms and conditions as specified in the corresponding bibliographic description in the repository

Publisher copyright

(Article begins on next page)

28 November 2026

Journal of Cleaner Production 503 (2025) 145382

Contents lists available at ScienceDirect

Journal of Cleaner Production

journal homepage: www.elsevier.com/locate/jclepro

Adsorption model for biogas purification: A design tool for solid oxide fuel cells applications

Elena Rozzi [a,b,*], Marta Gandiglio [a], Andrea Lanzini [a,b], Massimo Santarelli [a]

[a] Department of Energy, Politecnico di Torino, Corso Duca degli Abruzzi 24, 10129, Torino, Italy
[b] Energy Center Lab, Politecnico di Torino, Via Paolo Borsellino 38/16, 10138, Torino, Italy

ARTICLE INFO

Handling Editor: Panos Seferlis

Keywords:
Biogas cleaning
Techno-economic analysis
Adsorbent material
Adsorption model
Lead-and-lag layout
Fuel cells

ABSTRACT

With biogas production projected to exceed 35–45 billion cubic meters by 2030, addressing the critical challenge of biogas purification to allow its exploitation through the best-in-class technology available, the solid oxide fuel cell (SOFC), while preserving their durability, is essential. This study investigates the decontamination aspects related to the energy option of SOFCs fueled by biogas, a highly efficient and sustainable solution for renewable energy generation. We have developed a flexible and cost-effective biogas cleaning unit capable of removing harmful sulfur-based impurities. A novel adsorption model was created to predict contaminant concentration profiles, supporting the design of scalable cleaning units. Our comprehensive techno-economic analysis reveals that in 3-kW systems, capital and operational expenditures for SOFCs account for 56–70 % of the levelized cost of electricity (LCOE), with biogas cleaning systems constituting 30–37 % in single-vessel configurations and 35–44 % in lead-and-lag setups. In 100-kW systems, economies of scale reduce SOFC investment costs, while the impact of the biogas cleaning system becomes more pronounced. Sensitivity analysis indicates that variations in sorbent costs significantly affect LCOE, with lead-and-lag configurations offering advantages in sorbent utilization and operational efficiency. Overall, our findings indicate that biogas-SOFC systems obtain a competitive LCOE, below 0.32 €/kWh for 3-kW systems and below 0.12 €/kWh for 100-kW systems. This highlights their viability as a cleaner, high-efficiency alternative to conventional combustion technologies for decentralized energy production.

Abbreviations

BT	Breakthrough
CAPEX	Capital Expenditure
COS	Carbonyl Sulfide
DMS	Dimethyl Sulfide
GHSV	Gas Hourly Space Velocity
ICE	Internal Combustion Engines
LCOE	Levelized Cost of Electricity
LDF	Linear Driving Force
OPEX	Operational Expenditure
PDE	Partial Differential Equation
PSA	Pressure Swing Adsorption
RMSE	Root Mean Square Error
SOFC	Solid Oxide Fuel Cell
VPSA	Vacuum Pressure Swing Adsorption

1. Introduction

Over the past two decades, global biogas production has grown rapidly due to increasing demand for sustainable energy and efforts to mitigate greenhouse gas emissions. According to EBA (2022), combined production of biogas and biomethane is projected to more than double from the current 18.4 billion cubic meters (bcm) to 35-45 bcm by 2030, potentially reaching 95-167 bcm by 2050. This growth includes both medium to large-scale plants for biomethane upgrading and smaller decentralized plants (<50 m^3/h biogas production capacity), which are expected to remain critical (~15 % of output) for local heat and power generation, particularly in agricultural settings.

Although internal combustion engines (ICEs) are widely used for electricity generation, they typically exhibit low electrical efficiency (30–35 %) in small-to medium-scale operations. Solid oxide fuel cells (SOFCs) offer a promising alternative, achieving electrical efficiencies above 55 % even in small-scale applications (Gandiglio et al., 2020a),

* Corresponding author. Department of Energy, Politecnico di Torino, Corso Duca degli Abruzzi 24, 10129, Torino, Italy.
E-mail address: elena.rozzi@polito.it (E. Rozzi).

https://doi.org/10.1016/j.jclepro.2025.145382
Received 6 December 2024; Received in revised form 14 February 2025; Accepted 24 March 2025
Available online 24 March 2025
0959-6526/© 2025 The Authors. Published by Elsevier Ltd. This is an open access article under the CC BY-NC-ND license (http://creativecommons.org/licenses/by-nc-nd/4.0/).

and producing far lower nitrogen oxides (NO_x), sulfur oxides (SO_x), and particulate matter (PM) emissions (Gandiglio et al., 2020b).

Despite these technical advantages, high costs – up to 10,000 €/kW in small installations (Samanta et al., 2023) – remain a significant barrier to SOFC widespread adoption. Additionally, biogas purification is critical for SOFC operation. Sulfur-based compounds such as hydrogen sulfide (H_2S), carbonyl sulfide (COS), methanethiol (CH_4S) (Pera et al., 2024), and dimethyl sulfide (DMS) (Calbry-Muzyka et al., 2022) are especially detrimental, requiring H_2S levels to be reduced below 1 ppm (Lanzini et al., 2017).

Several biogas cleaning technologies have been developed, including water scrubbing, cryogenic separation, chemical and physical absorption, pressure swing adsorption, and membrane technologies (Paglini et al., 2022). For small-to medium-scale biogas plants, adsorption-based approaches using activated carbon, metal oxides, and zeolites are particularly appealing (Gandiglio, 2022), especially when sorbents are impregnated with transition metals, basic compounds (e.g., KOH, NaOH), or oxidizing agents (e.g., $KMnO_4$) (Coppola and Papurello, 2019).

This study represents one of the outcomes of the European Waste2-Watts project (W2W, 2022), which aimed to develop low-cost biogas cleaning units for high-efficiency fuel cells, focusing on small and medium-sized farms. An extensive experimental campaign at Politecnico di Torino (Italy), ENEA (Italy), and the Paul Scherrer Institute (Switzerland) tested various sorbent materials under variable conditions (aerobic/anaerobic environments, different humidity levels) to identify the most effective solutions.

Numerous studies have focused on the experimental analysis of adsorption capacities and the techno-economic assessment of biogas-SOFC systems. Duma et al. (2024) provided a comprehensive review of using metal-organic frameworks as sorbents for biogas cleaning, while Papurello et al. (2015a) used proton transfer reaction-mass spectrometry to characterize the adsorption behavior of sorbent materials able to remove propanethiol, butanethiol, methanethiol, and hydrogen sulfide from real OFMSW plant, focusing on the evaluation of breakthrough curves and optimization of filter configurations for selective removal. In contrast, Papurello et al. (2015b) investigated the overall gas clean-up efficiency of commercial sorbent materials for biogas upgrading, highlighting the need for a multi-stage filtration system to ensure biogas quality for SOFC applications.

Past research has examined the adsorption characteristics of sorbent under various operating conditions. The performance of various sorbent materials under different operating conditions has been extensively studied, including the effects of temperature, pollutant concentration, and relative humidity (Papurello et al., 2016), as well as bed height and dwell time (Papurello et al., 2020). Santoni et al. (2024) assessed both the operational performance and the physical properties of different sorbent materials, including surface area, pore size distribution, and functionalization compounds. Similarly, Molino et al. (2022) designed and tested an adsorption bed with activated carbons for biogas purification, focusing on the optimization of surface area and pore structure to enhance contaminant removal efficiency. Studies have also focused on optimizing surface area and pore structure for enhanced contaminant removal. Papurello et al. (2018) investigated the physical activation of waste-derived materials for biogas cleaning, analyzing how surface area and pore size distribution affect the adsorption capacity of hydrogen sulfide. Awe et al. (2017) conducted a comprehensive review on the removal of hydrogen sulfide from various industrial gas, emphasizing the role of sorbent material properties, such as surface areaand functional groups, in determining adsorption performance.

Costa et al. (2020) investigated the adsorption capacity of hematite-based sorbents before and after regeneration, while Micoli et al. (2014) assessed the performance of zeolites functionalized with Cu and Zn. Furthermore, Calbry-Muzyka et al. (2019) proposed a two-stage cleaning unit designed to address sulfur-based compounds and siloxanes. Lastly, Gandiglio (2022) conducted an evaluation of an industrial-scale biogas purification system aimed at the deep removal of impurities as part of the DEMOSOFC project.

Nevertheless, modeling of purification units is less developed. While Yoon and Nelson (1984) introduced a simplified theoretical model addressing the adsorption and breakthrough of contaminants, more recent work by Papurello et al. (2019a) conducted a comparative analysis of two predictive models for sorbent material replacement in a gas cleaning unit. The first, the Wheeler-Jonas model, employes a simplified equation based on macroscopic parameters. The second model is a one/dimensional dynamic adsorption model, which relies on partial differential equations to account for mass balance within the reactor, gas transport between gas bulk and sorbent particles, and the accumulation of adsorbed gas within the porous structure of the sorbent, following the Langmuir non-linear isotherm. Predictions from both models were validated with experimental observations to assess their accuracy. The most suitable isotherm for estimating sorbent adsorption capacity was further explored in (Papurello et al., 2019b), where Langmuir, Freundlich, Dubinin-Radushkevich, and Temkin isotherm equations were compared in terms of their ability to predict sorbent performance. Based on relative errors compared with experimental data, the Langmuir and Dubinin-Radushkevich equations were found to best represent the adsorption capacity of siloxane molecules within carbon-based materials. Moreover, a two-compound competitive adsorption model was proposed (Papurello et al., 2019c) and validated using experimental data.

Cherif (2016) also implemented a dynamic model of breakthrough curves for hydrogen sulfide adsorption onto activated carbon, highlighting the analytical challenges due to long simulation time and the need for small timesteps to avoid calculation divergence. Similar models have also been developed for carbon capture adsorption processes. Li et al. (2018) explored numerical simulations of CO_2 capture by adsorption, focusing on improving adsorbent performance and optimizing engineering processes. This study reviewed key mathematical models - covering adsorption kinetics, equilibrium, heat transfer, and pressure drop - to simulate and predict CO_2 adsorption in fixed-bed adsorbent columns. These models were validated through case studies of CO_2/N_2 mixtures, demonstrating their efficacy in optimizing adsorption unit performance. Lopes et al. (2011) proposed a mathematical model for simulating one-column vacuum pressure swing adsorption (VPSA) and PSA processes for hydrogen purification. This comprehensive model incorporates adsorption kinetics, mass and heat transfer, and pressure drop calculations. Solved using finite element methods in gPROMS, the model was tested with various cycle configurations and operational conditions. Comparisons with experimental data for multicomponent gas mixtures and different step sequences confirmed the model's accuracy in predicting process performance parameters such as purity, recovery, and productivity.

1.1. Novelty and contribution

Despite significant advancements in the modeling and analysis of biogas purification systems, critical gaps remain in the literature. Many existing models lack transparency in their formulation, making them difficult to replicate, while others omit explicit parameter values, limiting their applicability for large-scale system design. Although some studies have explored adsorption dynamics, few have developed robust models capable of accurately scaling cleaning units performance for industrial applications. Furthermore, the complexities associated with multi-vessel configurations, particularly those designed for continuous operation such as lead-and-lag setups, have not been thoroughly investigated.

This study presents a techno-economic assessment of biogas-SOFC systems at 3-kW and 100-kW scales, representative of small-to medium-sized agricultural and industrial applications. A key contribution is the development of a robust mathematical adsorption model that not only extrapolates experimental results but also serves as a design tool for

scaling up cleaning units. The model, described in detail in the methodology section, predicts transient contaminant concentration profile by dynamically adjusting to variations in feed concentration, contaminant types, flow rates, sorbent material, and reactor volume. Unlike previous works, the parameters and assumptions in this study are rigorously documented, ensuring full reproducibility and practical usability for system designers optimizing biogas purification for SOFC applications.

To assess the impact of different cleaning unit layouts, the study evaluates two distinct reactors configurations for H_2S removal. The first employs a single vessel, in which sorbent replacement is triggered once the H_2S concentration reaches 1 ppm, the threshold required to prevent SOFC catalyst degradation. The second configuration introduces a lead-and-lag setup which consists of two reactors in series, allowing for continuous operation. This approach ensues uninterrupted purification by switching reactors when sorbent in the first vessel is exhausted (Papadias et al., 2012). This novel two-reactor model maximizes sorbent utilization, avoiding operational interruptions and reducing material waste. The equivalent cumulative concentration method introduced in this study further enhances computational accuracy and efficiency, enabling better predictive modeling of sorbent behavior in multi-stage configurations.

Although biogas contains multiple contaminants - including siloxanes, volatile organic compounds, and halogenated compounds - the focus of this study is on H_2S removal, as it is the dominant limiting factor in the design of purification systems. Unlike other impurities, H_2S is typically present at significantly higher concentrations, ranging from 100 to 1000 ppm, making it the primary driver of sorbent consumption. Additionally, SOFCs have stringent tolerances for H_2S, requiring its concentration to be reduced below 1 ppm to prevent irreversible poisoning of the fuel cell catalyst. While other contaminants require filtration steps tailored to their chemical properties, they do not necessarily dictate the overall system design to the same extent as H_2S. The methodology developed in this study, however, is highly adaptable and can be extended to model the competitive adsorption of multiple contaminants, thereby broadening its applicability to more complex biogas purification scenarios.

Beyond its contributions to adsorption modeling, this study underscores the role of biogas-SOFC integration in improving the sustainability of power generation. Compared to conventional internal combustion engines, SOFCs offer higher electrical efficiency, typically reaching values between 50 % and 65 %, whereas ICEs operate in the 30–35 % range. Additionally, SOFCs nearly eliminate pollutant emissions such as NO_x, SO_x, and particulate matter, since they operate electrochemically rather than through combustion. The lead-and-lag configuration proposed in this study further enhances sustainability by maximizing sorbent utilization and minimizing material waste, thereby reducing the environmental footprint of the biogas purification process.

The findings of this study provide valuable insights for improving the economic feasibility of biogas-SOFC systems by balancing capital and operational expenditure trade-offs, refining LCOE estimations, and exploring scalable gas cleaning solutions. Notably, while the model is primarily focused on H_2S absorption, it can be easily adapted for other applications, such as CO_2 capture and hydrogen purification, thereby broadening its applicability in various gas cleaning scenarios.

The methodology is detailed in Section 2, where the adsorption model, layout configurations, and economic assessment calculations are presented. Section 3 discusses the results and includes a sensitivity analysis of economic parameters. Finally, Section 4 concludes the study with key findings and implications for future research.

2. Materials and methods

In this study, we model the process of biogas cleaning process using an adsorption unit to power a solid oxide fuel cell. The focus on H_2S is representative of typical scenarios in agricultural settings, where other contaminants are usually found only in trace amounts, as highlighted in the literature (Calbry-Muzyka et al., 2022).

The process flow is illustrated in Fig. 1. The biogas, primarily containing sulfur contaminants such as H_2S, is first pre-treated in a condenser to remove water vapor. This step is crucial because the presence of moisture could compromise the performance of sorbent materials used to remove hydrogen-based contaminants, and moisture can lead to corrosion or damage to the components of the adsorption column and the SOFC system (Gandiglio et al., 2020b). Once the biogas is dried, it enters the adsorption column, where the contaminants are adsorbed by the sorbent material, reducing the contaminant concentration to levels suitable for the SOFC. Finally, the clean biogas is fed into the fuel cell, where electricity is generated.

The methodology presented in this section evaluates the cleaning performance under real biogas plant operational conditions. It is divided into three main parts: the adsorption model based on partial differential equation (Section 2.1), the layout configurations for the cleaning unit operation (Section 2.2), and an economic analysis comparing different solutions in terms of levelized cost of electricity (Section 2.3).

2.1. Adsorption model

The performance of sorbents under real biogas plant operational conditions was simulated through a mathematical adsorption model based on a partial differential equation (PDE). This model describes the mass balance in the gas bulk phase, accounting for the following factors (Eq. (1)): i) $\frac{\partial C_i}{\partial t}$ represents the change in gas concentration over time within the packed-bed reactor; ii) $\frac{\partial(C_i\, u)}{\partial x}$ describes the convective mass transfer; iii) $\frac{1-\varepsilon_b}{\varepsilon_b}\rho_{bulk}\frac{\partial q_i}{\partial t}$ represents the rate of gas adsorption in the material due to catalyst reaction; and iv) $D_{ax}\frac{\partial^2 C_i}{\partial x^2}$ captures the molecular diffusion of gas through the reactor (Papurello et al., 2019a).

$$\frac{\partial C_i}{\partial t}+\frac{\partial(C_i u)}{\partial x}+\frac{1-\varepsilon_b}{\varepsilon_b}\rho_{bulk}\frac{\partial q_i}{\partial t}-D_{ax}\frac{\partial^2 C_i}{\partial x^2}=0 \quad [1]$$

The numerical solution of the PDE is computed discretizing the continuous variables of time (∂t) and space (∂x), transforming Eq. (1) into a system of algebraic equations that can be handled computationally (Eq. (2)).

$$\frac{C_i[n+1]-C_i[n]}{\Delta t}+\frac{u(C_i[n+1]-C_i[n-1])}{2\Delta x}+\frac{1-\varepsilon_b}{\varepsilon_b}k_i\rho_{bulk}\left(q_{eq,i}-q_i\right)-D_{ax}\frac{C_i[n+1]-C[n]+C[n-1]}{\Delta x^2} \quad [2]$$

The temporal derivative of gas concentration is discretized using the forward difference method to estimate the concentration at the next step ($C_i[n+1]$) based on the current concentration ($C_i[n]$). The convective term is approximated using a central difference scheme, averaging concentrations at adjacent grid points for a more accurate estimate in cases of smooth convective flow. The diffusion term is discretized using a second-order central difference method, effective for isotropic diffusion processes.

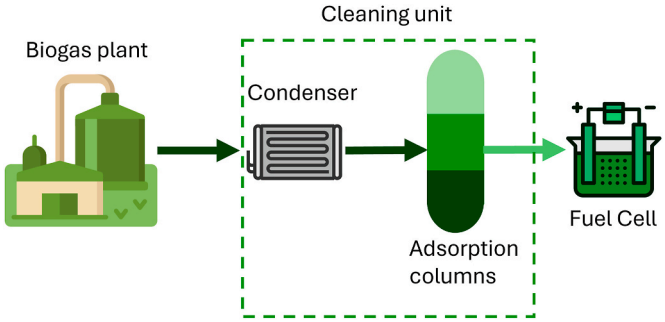

Fig. 1. Schematic configuration of the plant layout.

The gas interstitial velocity (u) is evaluated using Eq. (3), based on the volume flow rate (Q), the reactor area (A), and the bed void fraction (ε_b). The volume flow rate is expressed as a function of the gas hourly space velocity ($GHSV$) and the volume of the porous material ($V_{sorbent}$) as per Eq. (4). The bed void fraction, which identifies the void volume within the sorbent material (pores) and between the material particles (or pellets) is calculated using Eq. (5) based on the sorbent mass ($m_{sorbent}$), volume ($V_{sorbent}$) and skeleton density ($\rho_{skeleton}$).

$$u = \frac{Q}{A \cdot \varepsilon_b} \quad [3]$$

$$Q = GHSV \cdot V_{sorbent} \quad [4]$$

$$\varepsilon_b = \frac{m_{sorbent}}{V_{sorbent} \cdot \rho_{skeleton}} \quad [5]$$

In Eq. (2), ρ_{bulk} is the sorbent bulk density, q_i is the sorbed mass, and D_{ax} is the axial diffusivity, evaluated according to Eq. (6) as a function of the Schmidt number Sc, the Reynolds number Re, the molecular diffusivity D_m and the bed void fraction ε_b as proposed by Wakao and Funazkri (1978).

The Schmidt number depends on the kinematic viscosity ν (Eq. (9)) and the molecular diffusivity D_m (Eq. (10)) (Ratnakar and Dindoruk, 2022).

$$D_{ax} = \frac{D_m}{\varepsilon_b}(20 + 0.5\, ScRe) \quad [6]$$

$$Sc = \frac{\nu}{D_m} \quad [7]$$

$$Re = \frac{\varepsilon_b u d_p}{\nu} \quad [8]$$

$$\nu = \sum \frac{x_i\, \mu_i}{\rho_i} \quad [9]$$

$$D_m = \frac{k_B T}{6\pi\sigma \sum x_i \mu_i} \quad [10]$$

Here, x_i represents the contaminant mole fraction, μ_i is the dynamic viscosity of the species i, ρ_i is the species density, k_B is the Boltzmann's constant, and σ is the molecular radius of the gas.

The rate of gas absorption in the material is evaluated based on a mass balance equation within particles, depicted by the linear driving force (LDF) approximation, where the equilibrium adsorption capacity $q_{eq,i}$ is defined according to Langmuir isotherm equation (Eq. (11)) (Chauveau et al., 2013).

$$q_{eq,i} = q_{i,sat}\frac{K_L C_i}{1 + K_L C_i} \quad [11]$$

Where K_L is the Langmuir mass transfer coefficient, determined as a fitting parameter of the experimental curve, C_i is the contaminant concentration, and $q_{i,sat}$ is the adsorbent mass at saturation, extrapolated from experimental data.

The overall mass transfer coefficient k_i is computed according to Eq. (12) (Li et al., 2018).

$$k_i = \left(\frac{r_p}{3k_f}\frac{q_{eq_i}\rho_{ads}}{C_i} + \frac{r_p^2}{N_{ads}D_e}\frac{q_{eq_i}\rho_{ads}}{C_i\varepsilon_b} + \frac{r_c^2}{15D_{\mu i}} + \frac{r_p^2}{15D_{sup}}\right)^{-1} \quad [12]$$

The terms in Eq. (12) account for various diffusion processes:

1. The first term represents Knudsen diffusion, which defines the mass transfer due to collisions with the pore surface. This contribution decreases as the macroparticle radius (r_p) of sorbent particles (or pellets) is reduced. Additionally, it decreases at lower pressure due to the reduction of the adsorbed density (ρ_{ads}), which is assumed to be the density of the contaminant in its liquid state. The external fluid resistance k_f can be expressed as per Eq. (13).

$$k_f = \frac{Sh \cdot D_m}{2r_p} \quad [13]$$

Where Sh is the Sherwood number evaluated according to the empirical equation Eq. (14) (Wakao and Funazkri, 1978), as a function of the Schmidt number Sc and the Reynolds number Re.

$$Sh = 2 + 11Sc^{1/3} + Re^{0.6} \quad [14]$$

2. The second term of Eq. (12) represents the effective diffusion contribution, which is the mass transfer due to molecular interaction in the pores. The mass transfer increases with decreasing macroparticle radius and increasing effective molecular diffusivity (D_e). N_{ads} is a constant value equal to 15 is the sorbent shape is a sphere (particles) and 8 for cylinder shape (pellets) (Patton et al., 2004).

The effective molecular diffusivity (Eq. (15)) is computed as a function of the total molecular diffusion (Eq. (16)) and the Knudsen diffusion (Eq. (17)) which represents the collision between molecules and pore wall (Ratnakar and Dindoruk, 2022), The total molecular diffusivity combines the molecular diffusivity D_m, and the corrected diffusivity for a gas in a gas mixture $D_A^{'}$ (Eq. (18)), which is computed as a function of the binary diffusion coefficient as per the Slattery and Bird's equation (Eq. (19)) (Cherif, 2016).

$$D_e = \left(\frac{1}{D_{mt}} + \frac{1}{D_{ki}}\right)^{-1}\frac{\varepsilon_b}{\tau} \quad [15]$$

$$D_{mt} = \left(\frac{1}{D_A^{'}} + \frac{1}{D_m}\right)^{-1} \quad [16]$$

$$D_{ki} = 9,700 r_{mp}\sqrt{\frac{T}{PM}}\cdot 10^{-4} \quad [17]$$

$$D_A^{'} = \frac{1 - y_A}{\frac{y_B}{D_{AB}} + \frac{y_C}{D_{AC}} + \frac{y_D}{D_{AD}} \cdots} \quad [18]$$

$$D_{AB} = a\frac{\left(P_{c,pollutant}P_{c,i}\right)^{\frac{1}{3}}\left(T_{c,pollutant}T_{c,i}\right)^{\frac{5}{12}}\left(\frac{1}{PM_{pollutant}} + \frac{1}{M_i}\right)^{0.5}}{P} \cdot \left(\frac{T}{\sqrt{T_{c,pollutant}T_{c,i}}}\right)^{b} \quad [19]$$

$$\tau = \frac{\varepsilon_b}{1 - (1 - \varepsilon_b)^{\frac{2}{3}}} \quad [20]$$

Where τ is the tortuosity evaluated as per Eq. (20) (da Silva et al., 2022), r_{mp} is the macropore radius, $y_{A,B,C\ldots}$ are the species mole fractions, T is the absolute temperature, P is the absolute pressure, T_c is the critical temperature, P_c is the critical pressure, $M_{pollutant/i}$ is the molecular weight of the species, a and b are two dimensionless empirical coefficients equal to $2.745{\cdot}10^{-4}$ and 1.823 if the two species are nonpolar gasses, $3.64{\cdot}10^{-4}$ and 2.334 if one of the two gases is polar.

The term $\frac{q_{eq_i}\rho_{ads}}{C_i\varepsilon_b}$ represents the capacity of solute in porous bed, i.e., the ability of the particles of the porous bed to adsorb solute, relative to the concentration of the solute in the liquid phase flowing through the porous bed.

3. The third term of Eq. (12) represents the molecular diffusion in micropores (Poiseuille diffusion) which depends on the micropore diffusion coefficient ($D_{\mu i}$) and the micropore radius of the sorbent material (r_c), that can be neglected in this application (Farooq and Ruthven, 1990), while the last term represents the superficial diffusivity in pores which increase with decreasing superficial diffusion coefficient (D_{sup}). The micropore and the superficial diffusion coefficients are evaluated

Table 1
Input parameters for the adsorption model.

Variables	Value	Units	Description
T	303	K	Gas temperature
P	1	bar	Atmospheric pressure
k_B	1.380649×10^{-23}	J/K	Boltzmann constant
T_{b,H_2S}	212.87	K	Boiling temperature of H_2S
ρ_{bulk}	420	kg/m^3	Bulk density of the adsorbent
$\rho_{skeleton}$	545.4	kg/m^3	Skeleton density of the sorbent
r_{mp}	2.9×10^{-9}	m	Pore radius of the sorbent
r_c	3.347×10^{-10}	m	Micropore radius from BET data
r_p	1.5×10^{-3}	m	Macroparticle radius
σ	360×10^{-12}	m	Pollutant molecular radius
$q_{i,sat}$	0.3587	m^3/kg	Maximum adsorption capacity from BET isotherms
PM_{H_2S}	34.081×10^{-3}	kg/mol	Molecular weight of pollutant
PM_{CH_4}	16.0425×10^{-3}	kg/mol	Molecular weight of CH_4
PM_{CO_2}	44.0095×10^{-3}	kg/mol	Molecular weight of CO_2
PM_{O_2}	31.9988×10^{-3}	kg/mol	Molecular weight of O_2
PM_{N_2}	28.0134×10^{-3}	kg/mol	Molecular weight of N_2
PM_{H_2O}	18.0153×10^{-3}	kg/mol	Molecular weight of H_2O
ρ_{ads}	57.9	mol/m^3	Adsorbed density of H_2S at 303 K
μ_{H_2S}	1.2599×10^{-5}	Pa·s	Dynamic viscosity of pollutant
μ_{CH_4}	1.1232×10^{-5}	Pa·s	Dynamic viscosity of CH_4
μ_{CO_2}	1.5147×10^{-5}	Pa·s	Dynamic viscosity of CO_2
μ_{O_2}	2.0817×10^{-5}	Pa·s	Dynamic viscosity of O_2
μ_{N_2}	1.8028×10^{-5}	Pa·s	Dynamic viscosity of N_2
μ_{H_2O}	9.8553×10^{-6}	Pa·s	Dynamic viscosity of H_2O
P_{c,H_2S}	89.7	bar	Critical pressure of pollutant
P_{c,CH_4}	46.1	bar	Critical pressure of CH_4
P_{c,H_2O}	220.6	bar	Critical pressure of H_2O
P_{c,CO_2}	73.8	bar	Critical pressure of CO_2
P_{c,O_2}	50.4	bar	Critical pressure of O_2
P_{c,N_2}	33.9	bar	Critical pressure of N_2
T_{c,H_2S}	373.3	K	Critical temperature of pollutant
T_{c,CH_4}	190.6	K	Critical temperature of CH_4
T_{c,H_2O}	647	K	Critical temperature of H_2O
T_{c,CO_2}	304.1	K	Critical temperature of CO_2
T_{c,O_2}	154.6	K	Critical temperature of O_2
T_{c,N_2}	126 .2	K	Critical temperature of N_2
K_L	23.5577	–	Langmuir constant from fit of experimental data
Δx	0.001/0.01[a]	m	Spatial step size for the 3 kW and 100 kW scenarios
Δt	60	s	Time step size
$m_{sorbent}$	See Table 4	kg	Sorbent mass

[a] Due to computational expense, the simulation for the 100 kW system requires a higher spatial step size.

according to Eq. (21) and Eq. (22), respectively (Cherif, 2016).

$$D_{\mu i} = P\frac{r_c^2}{15\mu_i} \quad [21]$$

$$D_{sup} = 1.1\cdot 10^{-8} e^{\left(-5.32\ \frac{T_{b,pollutant}}{T}\right)} \quad [22]$$

$T_{b,pollutant}$ is the boiling temperature of the gas species, P is the pressure expressed in Pa.

Finally, the volume flow rate of the pollutant can be evaluated as a function of the computed concentration (in ppm_v) according to Eq. (23).

$$Q_{pollutant} = \frac{C_i}{10^6}\cdot Q_{tot} \quad [23]$$

The solution of the partial differential equation represents the evolution in time and space of the contaminant concentration $C = C(x,t)$ into the fixed bed and is solved imposing the boundary conditions at the domain borders (Eq.(24)–(27)).

$$C(x, t=0) = 0 \quad [24]$$

$$q(x, t=0) = 0 \quad [25]$$

$$C(x=0, t) = C_0 \quad [26]$$

$$\frac{\partial C}{\partial x}(x=L, t) = 0 \quad [27]$$

Eq. (24) and Eq. (25) impose the Dirichlet boundary conditions at initial time ($t = t_0$), i.e., the contaminant concentration at the adsorbed bed is null when the system starts the operation. Eq. (26) impose the Dirichlet boundary condition at the inlet of the reactor, i.e., the pollutant concentration at the reactor inlet is constant and equal to the initial concentration C_0. Finally, Eq. (27) imposes the Neumann boundary condition that states that the contaminant concentration is equal in the last two sections of the reactor.

The model's input parameters are summarized in Table 1. The pollutant considered in this analysis is the hydrogen sulfide (H_2S). The selected sorbent material is NORIT RGM3, an impregnated activated carbon that we have previously demonstrated to be effective in adsorbing COS, H_2S (Santoni et al., 2024) and other sulfur-based pollutant and volatile organic compounds (Papurello et al., 2014). Based on market analysis, this sorbent has been identified as a cost-effective solution, readily available within the supply chain, and suitable for scalability in larger systems. Supplement equations for gas mixture characterization are reported in Section S.1 of the Supplementary Material, while equations for the reactor design are presented in Section S.2.

The main model's output includes the outgoing contaminant concentration C_i and the loading profile q_i of the sorbent material at each time step.

Table 2
Parameters computed by the model.

Variable	Units	Description
Q_{H_2S}	m^3/s	Flow rate of pollutant gas
Q_{CO_2}	m^3/s	Flow rate of CO_2
Q_{O_2}	m^3/s	Flow rate of O_2
Q_{CH_4}	m^3/s	Flow rate of CH_4
Q_{N_2}	m^3/s	Flow rate of N_2
A	m^2	Reactor area
$GHSV$	1/h	Gas hourly space velocity
$V_{sorbent}$	m^3	Sorbent volume
$q_{eq,i}$	kg/m^3	adsorption capacity at equilibrium
C_i	mol/m^3	pollutant concentration
ε_b	–	Bed void fraction
τ	–	Tortuosity
u	m/s	Interstitial gas velocity
ν	m^2/s	Kinematic viscosity
k_i	1/s	Mass transfer coefficient
k_f	m/s	External fluid resistance
D_{CO_2}	m^2/s	Binary diffusion coefficient for CO_2 and pollutant
D_{CH_4}	m^2/s	Binary diffusion coefficient for CH_4 and pollutant
D_{H_2O}	m^2/s	Binary diffusion coefficient for H_2O and pollutant
D_{O_2}	m^2/s	Binary diffusion coefficient for O_2 and pollutant
D_{N_2}	m^2/s	Binary diffusion coefficient for N_2 and pollutant
D_m	m^2/s	Molecular diffusion coefficient
D_{mt}	m^2/s	Total molecular diffusivity
D_{ki}	m^2/s	Knudsen diffusivity in macropores
D_{sup}	m^2/s	Surface diffusion coefficient
$D_{\mu i}$	m^2/s	Poiseuille diffusion in micropores
D_e	m^2/s	Effective diffusivity in the reactor
D_{ax}	m^2/s	Axial diffusivity in the reactor
Sh	–	Sherwood number
Re	–	Reynolds number

The other computed parameters are listed in Table 2.

2.2. Layout configurations

In this study, two configurations were compared for managing H_2S contamination in SOFCs.

The first configuration (referred to as "single vessel") employed a single vessel, wherein the sorbent was replaced when the H_2S concentration in the outgoing flow reached 1 ppm, which aligns with the SOFC's tolerance for H_2S contamination (Lanzini et al., 2017). The outgoing contaminant concentration is evaluated based on the computed contaminant concentration at the outlet of the vessel, corresponding to the last point along the longitudinal direction, which is tracked at each time step.

In contrast, the second configuration (referred to as "lead-and-lag") operates with two reactors arranged in series under normal operation (Gandiglio, 2022). In this configuration, the lead reactor removes most of the contaminants, while the lag reactor acts as a polishing stage to ensure the biogas meets the required purity levels for SOFC operation. When the contaminant concentration downstream of the second reactor (lag vessel) approaches the breakthrough limit, the system switches to a parallel configuration to enable the replacement of the exhausted sorbent in the lead reactor without interrupting biogas flow to the SOFC. Once the replacement is completed, the system reverts to its original series configuration, with the newly regenerated reactor positioned as the lag reactor to ensure maximum protection of the SOFC unit.

This operational flexibility is achieved through the use of automated valves and real-time gas monitoring. Sampling points are positioned at the inlet and outlet of each reactor to continuously measure contaminant concentrations. These measurements allow the system to detect breakthrough events promptly and to coordinate the switching process efficiently. Therefore, by alternating between series and parallel configurations, the lead-and-lag setup ensures continuous biogas purification while minimizing downtime and maximizing sorbent efficiency. This flexibility makes it a robust solution for maintaining the operational reliability of biogas-fed SOFC systems.

This approach facilitates sorbent replacement without halting the operation of the SOFC unit and enhances the utilization of the sorbent materials by allowing them to be effectively used beyond the breakthrough point, thus maximizing the adsorbent capacity before replacement (see Fig. 2).

For the 2V model, at each timestep, the adsorption model assesses the concentration exiting the first reactor, starting from an initial condition of 1 ppm (breakthrough concentration) as this vessel contains the spent sorbent material. The outlet concentration from the first reactor serves as the inlet concentration for the second reactor. The working point of the second reactor is determined using an equivalent cumulative concentration ($C_{eq,cum}$) approach, which involves adjusting the timestep duration with the inlet concentration (Eq. (28)).

$$C_{eq,cum}(t) = C_{in}(t) \cdot \Delta t \quad [28]$$

The model subsequently identifies the concentration of the adsorption curve that corresponds to the cumulative mass of contaminants entering the second reactor. The concentration at the outlet of the second reactor is then determined from this curve, ensuring that the dynamics accurately reflect the contaminant input from the first reactor. For further details see Section S.3 of the Supplementary Material.

To optimize computational time, the outgoing contaminant concentration was initially computed for a range of inlet concentrations (from 1 to 1000 ppm, in increments of 5 ppm). Subsequently, for each timestep, the model identifies the adsorption curve nearest to the inlet concentration in the second reactor.

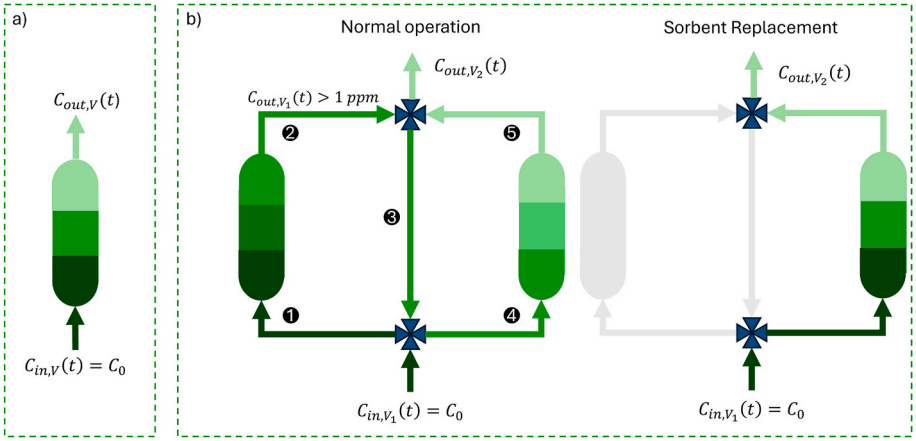

Fig. 2. Schematics of a) single vessel layout, b) lead-and-lag configuration, where two reactors operate in series under normal conditions and switch to a parallel configuration during sorbent replacement to ensure continuous operation.

Table 3
Economic parameters.

Parameter	Value	Refs.
SOFC CAPEX [€/kW]	Cost function 3 kW: 8000 €/kW 100 kW: 1850 €/kW	Rozzi et al. (2024)
SOFC OPEX [%]	2 %	Cigolotti and Genovese (2021)
SOFC replacement cost [%CAPEX]	40 %	Cigolotti and Genovese (2021)
SOFC stack lifetime [years]	8	Cigolotti and Genovese (2021)
SOFC efficiency [%]	55 %	Cigolotti and Genovese (2021)
SOFC capacity factor [%]	99 %	Gandiglio et al. (2020b)
SOFC start-up cost [€/h]	7	Comsos (2020)
Reactor vessel CAPEX [€/m^3]	Cost function 3 kW: 31,400 €/m^3 100 kW: 7850 €/m^3	Turton et al. (2012)
Heat exchanger CAPEX [€]	Cost function 3 kW: 830 € 100 kW: 3060 €	Turton et al. (2012)
Lifetime [years]	20	Oluleye and Hawkes (2020)
Sorbent cost [€/kg]	8	Rozzi et al. (2024)
Disposal sorbent cost [€/kg]	4.5	DEMOSOFC (2020)
Replacement and start-up time [h]	48	DEMOSOFC (2020)
Replacement labour [€]	400	–
Installation costs [%CAPEX]	30 %	Cigolotti and Genovese (2021)
Interest rate [%]	5 %	Rozzi et al. (2024)

Table 4
Setting parameters for experimental tests and real-case scenario.

Parameters	Test conditions	Real biogas simulation 3 kW	Real biogas simulation 100 kW
Flow rate [m^3/h]	0.04	0.5	18.3
Temperature [°C]		30	
H_2S inlet [ppm_v]	500	100–500 – 1000	
L/D ratio	3.76	1.7 (Gandiglio, 2022)	
Biogas composition (y_i)	CH_4:CO_2 50:50	CH_4:CO_2:N_2 56:42:2	
Sorbent mass [kg]	$14.05 \bullet 10^{-3}$	40	1460
Sorbent shape		Pellet	

2.3. Economic assessment

The economic comparison of the two cleaning unit layouts is conducted by evaluating the levelized cost of electricity (LCOE) for each configuration according to Eq. (29).

$$LCOE = \frac{\sum_{t=1}^{n} CAPEX_i + \sum_{t=1}^{n} OPEX_i}{\sum_{t=1}^{n} \frac{E_{gen}}{(1+r)^n}} \quad [29]$$

Where $CAPEX_i$, represents the total investment costs associated with the SOFC and the cleaning units, including the vessels containing the sorbent material and the condenser. The total investment cost is calculated by increasing the CAPEX of each component by 30 % to account for installation costs. In the lead-and-lag operation, the installation cost of the reactors is assumed to be equivalent to that of a single vessel, as the installation components remain unchanged.

$OPEX_i$ refers to the annual operational costs of these components, evaluated as a percentage of CAPEX. Additionally, the operational costs for the SOFC unit include stack replacement costs and start-up costs, which account for the management of the SOFC during shutdown and start-up events. OPEX associated with sorbent material covers the cost of the material itself, the disposal of the spent sorbent, and labor expenses for its replacement. The term E_{gen} denotes the annual electric energy generated by the fuel cell. The parameters r and n correspond to the interest rate and the expected lifetime of the plant, respectively.

The price of the sorbent material is set at 8 €/kg (Papurello et al., 2015a), while the costs associated with the SOFC are computed according to the cost function proposed by (Rozzi et al., 2024). The costs for the heat exchanger and sorbent vessels are derived from the cost functions detailed by Turton et al. (2012). A summary of the key economic assumptions is presented in Table 3.

The biogas supply cost is assumed to be zero, as the study considers waste-derived biogas from wastewater treatment plants and landfills, where biogas is a byproduct of the waste treatment process rather than a purchased commodity (MosayebNezhad et al., 2018). This aligns with common assumptions in techno-economic assessments of waste-to-energy systems, where the primary objective is waste management, and biogas utilization serves as an energy recovery strategy rather than a cost-bearing fuel source.

The reactor volume was assumed to be 10 % larger than the volume occupied by the sorbent material. In the single-vessel configuration, sorbent replacement is assumed to necessitate a 1-day SOFC shutdown. Contrariwise, in the lead-and-lag layout, the sorbent replacement does not result in any system shutdown.

The cost functions are reported in Section S.4 of the Supplementary Material.

3. Results and discussion

This section presents the findings of the adsorption model validation and its application to various operational scenarios. Initially, the model's accuracy was validated against experimental data under specific test conditions. Following validation, we examined the adsorption performance of different configurations - namely single vessel and lead-and-lag setups - across varying inlet H_2S concentrations. Finally, we conducted an economic assessment of the proposed solutions, focusing on the levelized cost of electricity in relation to system components and operational expenses.

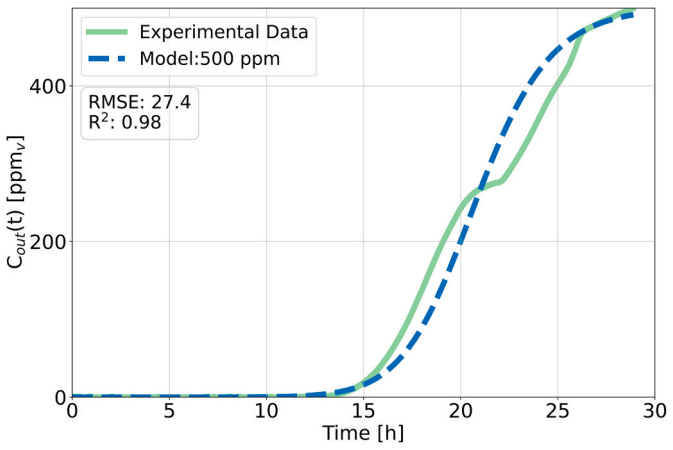

Fig. 3. Outgoing pollutant concentration from model results and experimental data with an inlet contaminant concentration of 500 ppm.

3.1. Adsorption model results

The adsorption model was first validated against experimental data using the test conditions outlined in Table 4. The experimental tests were conducted with an inlet H_2S concentration of 500 ppm and a biogas flow rate of 0.04 m^3/h, with a mixture of 50 % CH_4 and 50 % CO_2 (Santoni et al., 2024). The model fitting returns a Langmuir coefficient of 23.56. Once validated, the model was applied to real-case scenarios, adjusting input parameters as specified in Table 4 to represent a broader range of operational conditions typically found in real small-size biogas plants. For instance, the flow rate was increased to 0.5 and 18.3 m^3/h to simulate the operational scale of a 3-kW and 100-kW SOFC, respectively, in industrial applications. Additionally, the model was tested with varying H_2S concentrations (100, 500, and 1000 ppm) to reflect different contamination levels (Pera et al., 2024). The case studies considered in this work are based on biogas derived from wastewater treatment plants, which typically exhibits low variability in composition, with H_2S as the dominant contaminant. This is due to preliminary sulfur removal in the water treatment line with iron hydroxide, leading to relatively stable gas-phase concentrations (Gandiglio, 2022). The selected H_2S concentration values (100, 500, and 1000 ppm) represent upper-bound scenarios, ensuring a conservative approach for the design of the cleaning unit. By adopting these values, the model accounts for potential variations while maintaining robustness in sorbent performance predictions across different operational conditions.

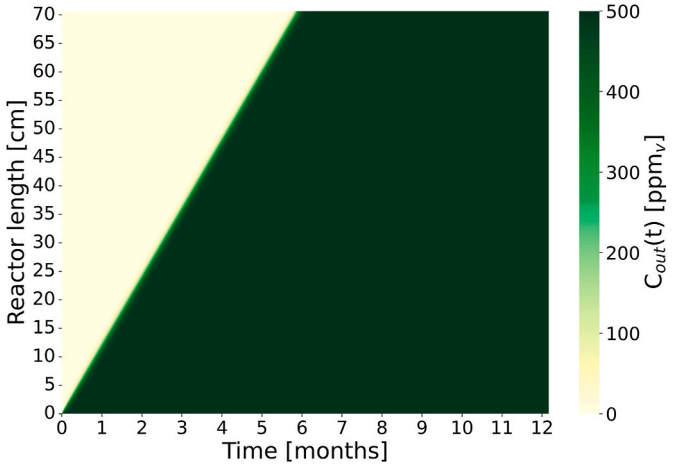

Fig. 4. H_2S concentration profile in a 3-kW reactor over one year, at 0.5 m^3/h biogas flow, 40 kg of sorbent, and 500 ppm inlet concentration.

The sorbent mass in the 100-kW scenario was adjusted to maintain the same gas hourly space velocity (GHSV) as in the 3-kW system (5.25 h^{-1}), despite the higher flow rate.

The CO_2 content in biogas, typically ranging from 40 % to 50 %, has a limited impact on SOFC performance. Unlike other fuel cell technologies, SOFCs can efficiently operate with raw biogas without requiring extensive CO_2 removal. While CO_2 slightly affects reforming reactions and fuel dilution, studies indicate that SOFC efficiency remains stable across a broad range of methane concentrations. Various CO_2 pretreatment strategies, such as pressure swing adsorption, membrane separation, and amine scrubbing, are available to enhance methane concentration, but they introduce additional costs and complexity, which may not always be justified.

Experimental results from a real biogas-fed SOFC plant (Gandiglio et al., 2024) demonstrate that SOFC efficiency remains stable between 50 and 55 %, even with methane concentrations ranging from 55 % to 70 %. Additionally, comparative studies of biogas-fed and natural gas-fed SOFC systems indicate that both exhibit equivalent performance (Gandiglio et al., 2024). These findings confirm that, for most decentralized SOFC plants, direct biogas utilization without CO_2 upgrading remains a technically and economically viable approach, eliminating the need for additional purification steps.

Fig. 3 shows the comparison between experimental data and model predictions for the outgoing H_2S concentration at an inlet concentration of 500 ppm. The adsorption curves at 100 and 1000 ppm were also evaluated at the same operational conditions. The model closely mirrors the experimental results, with an R^2 of 0.98 and a root mean square error (RMSE) of 27.4, confirming its accuracy under the test conditions.

While the overall agreement is strong, minor deviations are observed after breakthrough. In the initial phase following BT (15–20-h range), the experimental curve shows a steeper concentration increase than predicted by the model, indicating a slight underestimation of the contaminant release rate. However, at intermediate saturation levels, the trend reverses, and the model overestimates the outlet concentration. This behavior suggests that the adsorption front propagation in the real system may be influenced by local sorbent heterogeneities and mass Despite these minor differences, both experimental and simulated curves converge at full saturation, confirming the model's reliability in predicting overall system performance.

The model was then applied to real-case scenarios with varying operational parameters. Fig. 4 presents the concentration map of the H_2S contaminant inside the reactor, plotted as a function of both reactor length and time, providing insights into the spatial and temporal evolution of the adsorption process within the reactor. The figure corresponds to a 3-kW SOFC system operating with an incoming biogas flow rate of 0.5 m^3/h, with 40 kg of sorbent material in a single vessel configuration, and an inlet concentration of 500 ppm of H_2S.

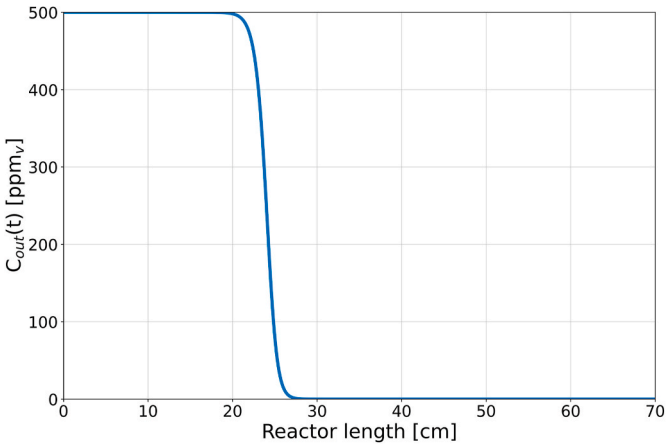

Fig. 5. H_2S concentration profile along the reactor length at a fixed time.

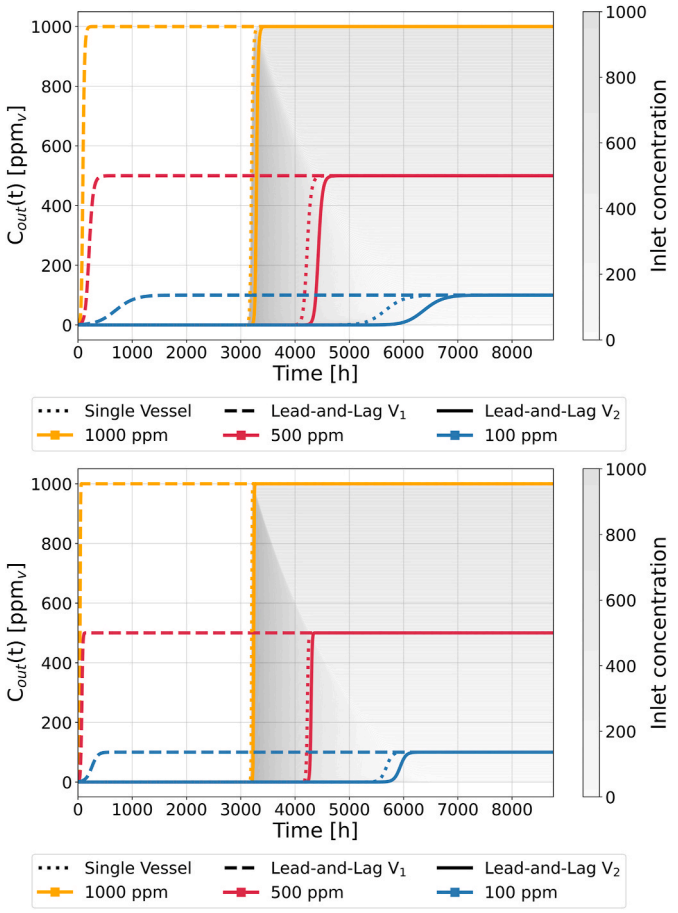

Fig. 6. Adsorption curves for 100, 500, and 1000 ppm inlet H_2S concentrations in a 3-kW system (0.5 m^3/h biogas flow rate, 40 kg sorbent mass; upper panel) and 100-kW system (18.3 m^3/h biogas flow rate, 1460 kg sorbent mass; lower panel). Dotted line: single vessel outlet. Dashed line: first vessel in lead-and-lag. Solid line: second vessel outlet. Gray curves: absorption profiles for inlet concentrations from 1 to 1000 ppm.

The vertical axis represents the reactor length, while the horizontal axis indicates time. The color gradient illustrates the H_2S concentration at different points along the reactor's length over time. Darker shades signify higher concentrations of H_2S. At the start of the process (month 0), the H_2S concentration is zero across the reactor length, indicating that the sorbent material is effectively removing the contaminant. The first portion of the reactor, where the sorbent is fresh, adsorbs all incoming H_2S, keeping the outlet concentration below 1 ppm. As time progresses, the sorbent material gradually saturates, and the H_2S concentration increases along the reactor length. Finally, the concentration of H_2S in the outlet stream rises significantly, reaching 500 ppm as the sorbent becomes fully saturated and can no longer effectively remove the contaminant.

The adsorption front propagates in a nonlinear manner, as the sorbent progressively saturates. This behavior becomes evident in Fig. 5, where the concentration profile at a fixed time (month 2) reveals a sharp drop from 500 ppm to near-zero within a short reactor length, confirming the intrinsically nonlinear nature of the adsorption process.

3.2. Adsorption performance comparison across configurations

Fig. 6 illustrates the adsorption curves for different inlet H_2S concentrations (100, 500, and 1000 ppm) in both single vessel and lead-and-lag configurations.

The gray curves represent the absorption profiles for a range of inlet contaminant concentrations (from 1 ppm to 1000 ppm, with steps of 5 ppm). These profiles are essential for calculating the outlet concentration from the second vessel in the lead-and-lag configuration, where the outlet from the first vessel serves as the inlet for the second one. The dotted lines show the outlet H_2S concentration from a single vessel system for the respective inlet concentrations. The dashed curves represent the outlet concentration from the first vessel in the lead-and-lag configuration, where breakthrough has already occurred. Initially, this vessel partially adsorbs the contaminant, but as the sorbent saturates, the outlet concentration approaches the inlet value. Finally, the solid line represents the outlet concentration from the second vessel in the lead-and-lag setup. The second vessel provides additional contaminant removal, even after the first vessel is saturated, extending the operational time and improving removal efficiency compared to the single vessel configuration. Further details on the adsorption kinetics

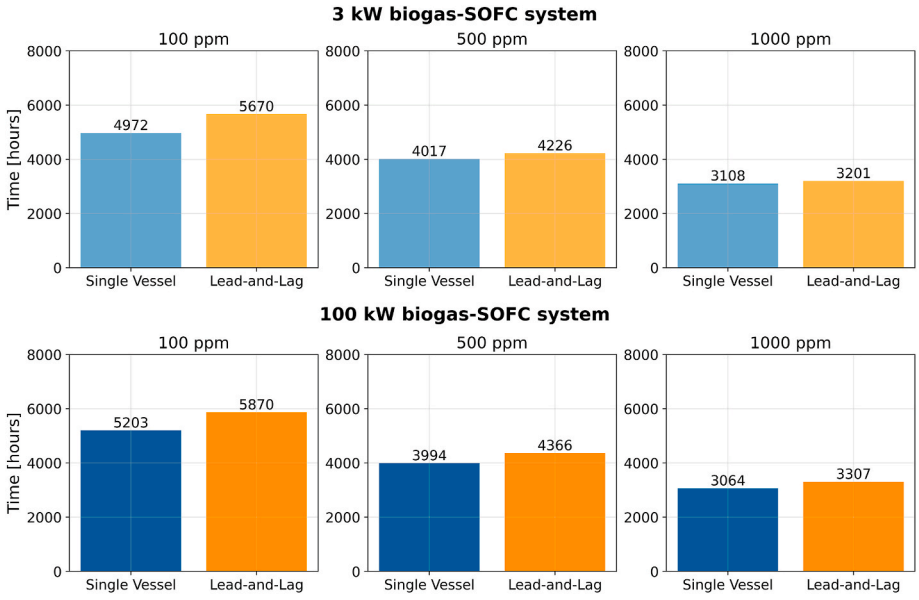

Fig. 7. Breakthrough time for the analyzed configurations. Blue bars refer to the single vessel configuration, orange bars to the lead-and-lag configuration. (For interpretation of the references to color in this figure legend, the reader is referred to the Web version of this article.)

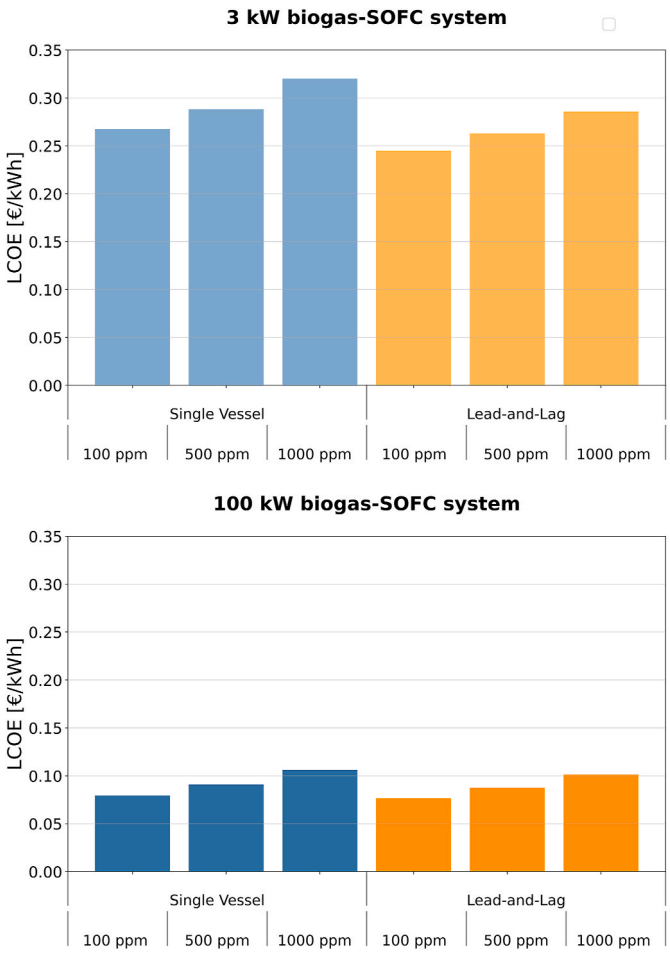

Fig. 8. Levelized cost of electricity for a 3-kW (*upper*) and 100-kW (*bottom*) biogas-SOFC system at different H_2S inlet concentrations with single vessel and lead-and-lag layout.

and the evolution of the outlet concentration profiles, particularly regarding the slope of the breakthrough curves and its dependence on the inlet H_2S concentration, are provided in Supplementary Section S.5.

Fig. 7 illustrates the breakthrough (BT) time for the configurations analyzed. As expected, the lead-and-lag setup demonstrates a longer BT time compared to the single-vessel configuration, reflecting its ability to maximize sorbent utilization and achieve higher adsorption capacity across all scenarios. No significant differences were observed between the 3-kW and 100-kW systems, with minor variations attributed to computational inaccuracies, likely due to different spatial step sizes used in the model to manage computational time constraints. In particular, for the 100-kW system, the larger spatial step (0.01 m in the 100-kW case compared to 0.001 m in the 3-kW case) introduces a numerical uncertainty in BT time estimation, especially at lower inlet concentrations. A slight reduction in BT time for the 100-kW system was expected. Despite maintaining the same GHSV, the larger system's scale increases the interstitial gas velocity, which in turn increases axial diffusivity. As demonstrated by Papurello et al. (2019a), this leads to a steeper adsorption curve and a reduction in BT time.

In both configurations, a lower inlet concentration results in a greater gain in BT time with the lead-and-lag setup. At 100 ppm, the gain is around 13–14 %, at 500 ppm it drops to 5–9 %, and at 1000 ppm, it ranges between 3 and 8 %. This occurs because higher concentrations lead to quicker saturation of binding sites (Zulkefli et al., 2017). The steeper BT-saturation curve at 1000 ppm indicates that the first adsorption column's effect is reduced, limiting the benefit period of the lead-and-lag configuration.

3.3. Economic assessment

The economic performance of the biogas-SOFC systems, as shown in Fig. 8, reveals a clear dependency of the LCOE on both the H_2S concentration in the biogas and the cleaning unit layout. For the 3-kW system, the LCOE ranges between 0.24 and 0.32 €/kWh, while for the 100-kW system, it varies from 0.08 to 0.11 €/kWh. These values are consistent with existing literature.

A comparison with international benchmarks from the IEA database (IEA, 2020) on biomass and biogas conversion shows that small-scale biomass-fired plants exhibit comparable or higher LCOE values. For example, small-scale biomass-fired power plants in Italy (450 kW) report an LCOE from 0.076 €/kWh to 0.289 €/kWh depending on assumptions on fuel costs. Similarly, large-scale biomass CHP plants in Denmark (177–358 MW) report an LCOE ranging from 0.095 to 0.170 €/kWh, reinforcing the competitive economic viability of SOFC-based systems, particularly at 100-kW scales.

A more direct comparison with biogas-based ICE and SOFC technologies is provided by Girola et al. Giarola et al. (2018), who evaluated different conversion technologies under three operational scenarios. Their study found that conventional ICEs exhibit lower LCOE values in the baseline case (0.104 €/kWh) compared to SOFCs (0.173 €/kWh). However, when optimized sludge pre-thickening is implemented, SOFCs achieve a 30–50 % reduction in LCOE, reaching 0.057 €/kWh, making them significantly more competitive. These findings align with our results, where the 100-kW SOFC system achieves LCOE values down to 0.08 €/kWh, demonstrating that advanced system designs and biogas upgrading strategies further improve economic feasibility.

Additionally, Ma et al. (2024) analyzed two biogas-fed SOFC systems with integrated purification and carbon capture and storage, reporting

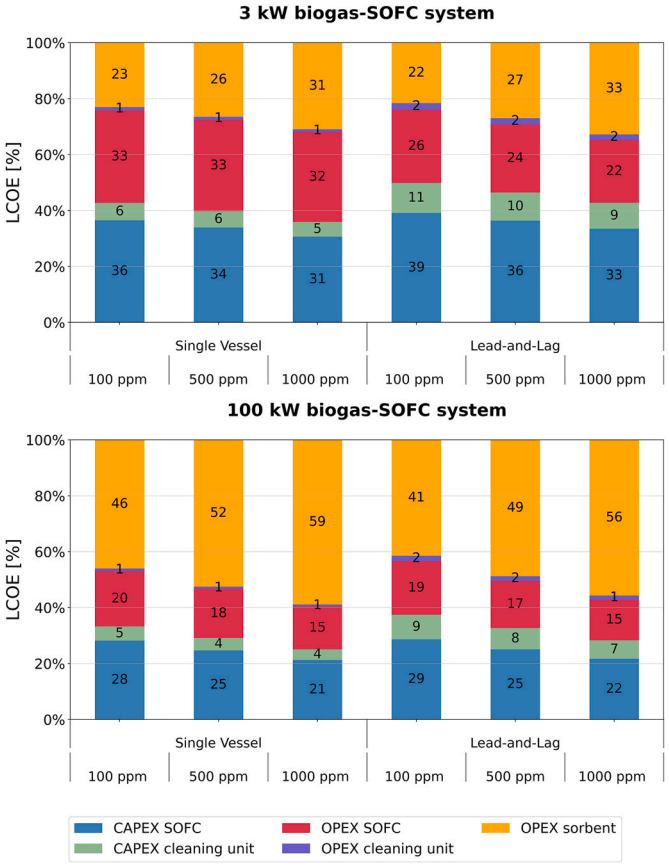

Fig. 9. Levelized cost of electricity breakdown for a 3-kW (*upper*) and 100-kW (*bottom*) biogas-SOFC system at different H_2S inlet concentrations with single vessel and lead-and-lag layout.

LCOE values between 0.150 and 0.168 €/kWh for a 20-kW system. While these values are slightly higher than those calculated for our 100-kW system, they highlight the cost trade-offs associated with additional CO_2 capture strategies. Their results also confirm that SOFC efficiency improvements (up to 65.5 %) significantly reduce LCOE, reinforcing the advantages of optimized biogas-SOFC integration.

A key observation is the increase in LCOE with higher H_2S concentrations, which results from the decreasing BT time of the sorbent (Fig. 7). As the BT time shortens, a larger amount of sorbent is required, thereby increasing operational costs. For instance, in the 3-kW system with a single vessel layout, the LCOE rises from 0.27 €/kWh at 100 ppm to 0.32 €/kWh at 1000 ppm, while in the lead-and-lag layout, it increases from 0.24 €/kWh to 0.29 €/kWh over the same concentration range, and a similar trend is observed for the 100-kW system.

The purification layout has a large impact on the overall system economics. The introduction of the lead-and-lag layout leads to a notable reduction in LCOE, decreasing by 9–12 % for the 3-kW system, compared to a more modest 4–5 % reduction for the 100-kW system. This difference is attributed to a 13–14 % reduction in the annual cost for the sorbent replacement in the lead-and-lag setup, although this benefit is partially offset by a 44–48 % increase in investment costs for the gas cleaning unit due to the additional reactor required.

Additionally, the system size plays a crucial role in cost reduction, as the larger 100-kW system consistently exhibits much lower LCOE values compared to the 3-kW system, demonstrating that significant economies of scale are achieved in larger installations.

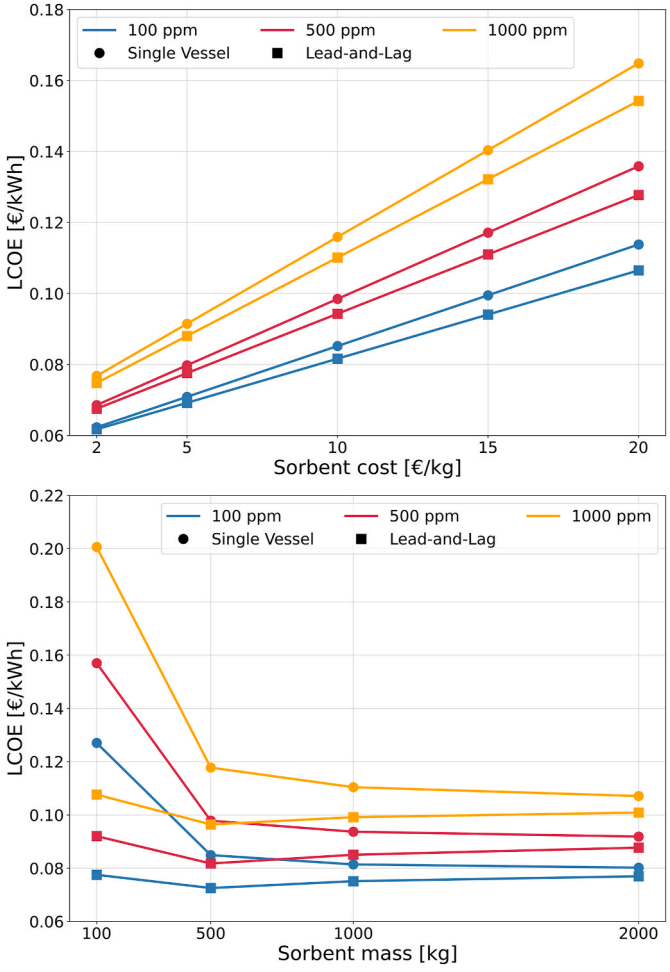

Fig. 10. Sensitivity analysis of the levelized cost of electricity for a 100-kW biogas-SOFC system as a function of i) sorbent cost (*upper*) and ii) sorbent mass (*bottom*), at different H_2S inlet concentrations with single vessel and lead-and-lag layout.

The cost breakdown of the 3-kW and 100-kW biogas-SOFC systems, shown in Fig. 9, provides deeper insight into the contribution of capital expenditure (CAPEX) and operational expenditure (OPEX) to the overall LCOE across the system components.

For the 3-kW system, the combined CAPEX and OPEX of the SOFC unit constitutes a substantial portion of the LCOE, ranging from 56 % to 70 % depending on the configuration and inlet H_2S concentration. This reflects the high unit cost of small-scale fuel cells, which constitutes a significant cost driver in this size range. By contrast, the CAPEX of the cleaning unit is considerably lower, accounting for 5–6 % of the LCOE in the single vessel configuration and increasing to 9–11 % in the lead-and-lag setup due to the added complexity of a second reactor. However, the OPEX of the cleaning unit - particularly the cost of the sorbent - plays a major role in operational costs. The sorbent costs alone account for 22–33 % of the LCOE.

For the 100-kW system, the benefits of economies of scale are pronounced. The contribution of the SOFC unit to the LCOE is notably reduced, ranging from 21 % to 29 %, a significant drop compared to the 3-kW system. The CAPEX of the cleaning unit is similarly low, accounting for 4–5 % of the LCOE in the single vessel configuration and rising to 7–9 % in the lead-and-lag setup. However, the OPEX of the cleaning unit - especially sorbent costs - dominates the operational costs. Sorbent costs alone range from 41 % to 59 % of the LCOE, with a clear increase as the inlet H_2S concentration rises. For instance, at 1000 ppm, the OPEX sorbent cost accounts for 59 % of the LCOE in the single vessel configuration and 56 % in the lead-and-lag setup. These cost breakdown shares align with those proposed in previous studies.

Papadias et al. (2012) conducted an economic analysis of a stationary fuel cell system, highlighting that advanced biogas cleaning technologies can significantly impact both capital and operational expenditures. Similarly, Wasajja et al. (2020) performed a techno-economic review of biogas cleaning technologies for small-scale off-grid SOFC applications, noting that gas cleaning unit could increase the system capital cost by 6–7 % and account for more than 40 % of the overall annual operating cost.

Further details on the breakdown of LCOE contributions are provided in Supplementary Section S.6, supporting the analysis of design trade-offs between the single vessel and lead-and-lag configurations.

3.4. Sensitivity analysis

To assess the economic robustness of the biogas-SOFC system, a sensitivity analysis was conducted on the 100-kW system, focusing on two key variables in the cleaning unit: the sorbent cost and the sorbent mass within the absorption reactor. The baseline sorbent cost, initially set at 8 €/kg, was varied across a range between 2 €/kg and 20 €/kg to evaluate its impact on the levelized cost of electricity (Gandiglio, 2022). Similarly, the sorbent mass within the reactor, originally fixed at 1460 kg, was adjusted to examine scenarios with mass ranging from 100 kg to 2000 kg of sorbent.

As shown in Fig. 10 on the left, the sensitivity analysis on sorbent costs demonstrates a clear trend: higher sorbent costs lead to an increase in the LCOE across all H_2S concentrations. This impact is particularly pronounced at higher sorbent costs, where the differences between the single vessel and lead-and-lag configurations become more significant. At lower sorbent costs (e.g., 2 €/kg), the difference in LCOE between the single vessel and lead-and-lag setups is relatively small (~2 %). However, as the sorbent cost rises, the lead-and-lag layout shows a greater economic advantage due to its improved sorbent utilization, which results in a reduced replacement frequency. This advantage becomes increasingly impactful at higher sorbent costs, where each replacement incurs a more substantial cost penalty. For instance, at a sorbent cost of 20 €/kg and an inlet concentration of 1000 ppm H_2S, the LCOE for the lead-and-lag setup is 0.154 €/kWh, compared to 0.165 €/kWh in the single vessel configuration, resulting in a 7 % reduction in LCOE.

Notably, while the LCOE values vary with H_2S concentration, the trend and the differences between the single vessel and lead-and-lag configurations remain similar across different concentrations.

Similarly, Fig. 10 on the right illustrates the sensitivity analysis on sorbent mass. The LCOE is higher at lower sorbent masses due to the need for more frequent replacements. Each replacement incurs not only the cost of new sorbent material, but also additional operational expenses related to labor and disposal. In the single vessel configuration, these costs are further compounded by the startup costs associated with the SOFC system after each replacement. As a result, at lower sorbent masses, the LCOE is consistently higher for the single vessel setup compared to the lead-and-lag configuration, with an increase of 64–86 %. The lead-and-lag design benefits from improved sorbent utilization, which helps to extend the time between replacements. This cost advantage of the lead-and-lag setup is observed consistently across all inlet contaminant concentrations, with similar patterns of LCOE variation regardless of concentration level. At higher sorbent masses (e.g., 1000 kg and 2000 kg), the LCOE stabilizes across both configurations, as the reduced frequency of replacements diminishes the impact of operational interruptions and disposal costs. The difference in LCOE between the layouts is 8–10 % for the 1000 kg cleaning unit and 4–6 % for the 2000 kg cleaning unit. The 100 kg scenario represents an extreme case, implying that the sorbent mass would need to be replaced every 7–12 days – an unrealistic frequency for actual plant operations.

3.5. Discussion on model performance

While this study focuses on H_2S removal, biogas contains other harmful contaminants, such as dimethyl sulfide, methanethiol, carbonyl sulfide, and siloxanes, which can also impact SOFC performance and operating costs. These compounds require additional purification steps, which may lead to increased sorbent consumption and replacement frequency, affecting both capital and operational expenditures. The economic impact of these contaminants depends on their concentration levels, removal efficiency, and the specific sorbent material used. Studies have shown that organosulfur compounds have lower adsorption rates compared to H_2S, potentially requiring longer residence times or specialized sorbents, increasing system complexity and cost. Similarly, siloxanes, commonly found in landfill-derived biogas, necessitate additional filtration stages, adding to investment and maintenance expenses.

The CO_2 content in biogas, typically ranging from 40 % to 50 %, has a limited influence on SOFC performance. SOFCs can efficiently utilize raw biogas without requiring extensive CO_2 removal. While CO_2 slightly affects fuel composition and reforming reactions, studies indicate that SOFC efficiency remains stable across a wide range of methane concentrations. Various pre-treatment strategies, such as pressure swing adsorption, membrane separation, and amine scrubbing, can be implemented to enhance methane concentration, but they introduce additional costs and system complexity, which may not always be warranted in decentralized applications.

Expanding the adsorption model to accommodate a broader range of contaminants requires consideration of multi-contaminant adsorption effects and adjustments to the model to account for different types of compounds. In gas mixtures, competitive adsorption effects must be considered, as different contaminants interact with the sorbent material, influencing adsorption capacity and breakthrough behavior. The Ideal Adsorbed Solution (IAS) approach is commonly employed to model such interactions, extending the Langmuir isotherm to multi-component systems. This method assumes that the adsorption equilibrium of a gas mixture behaves like an ideal solution of adsorbed species rather than independent adsorption events. Given that biogas purification often involves the removal of multiple contaminants - including siloxanes, volatile organic compounds, ammonia, and halogenated compounds - IAS-based approaches provide a more accurate representation of sorbent behavior compared to models that assume independent adsorption (Papurello et al., 2019c). Moreover, it is necessary to adjust the adsorption parameters to reflect differences in adsorption mechanisms. Each compound has unique adsorption characteristics depending on its molecular size, polarity, and chemical reactivity with the sorbent. For example, siloxanes are predominantly removed via physisorption, whereas ammonia and halogenated compounds may undergo chemisorption or catalytic decomposition on the sorbent surface. The adsorption affinity and maximum adsorption capacity must be determined experimentally for each sorbent-contaminant pair. In some cases, additional reaction mechanisms may need to be incorporated into the model, particularly for contaminants that undergo surface reactions or decomposition rather than simple adsorption. Future work should consider a multi-contaminant removal approach, integrating economic and adsorption models to quantify the cumulative effect of different impurities on LCOE and system performance.

In this study, biogas composition and operating conditions, including CO_2 content, water vapor presence, temperature, and pressure, were kept constant, as they were not the primary focus of the analysis. However, these parameters are fully integrated into the adsorption model, allowing flexible adjustments to simulate different operating scenarios and assess their impact on system efficiency. The assumption of constant temperature and pressure is reasonable in the context of most small-scale biogas plants, where fluctuations are minimal. Biogas flow rate was also considered constant, meaning that seasonal or daily variations in biogas production were not explicitly modeled. While such variations exist, they are relatively small in well-managed systems, making this a valid simplification for the purpose of designing the purification unit. Similarly, contaminant concentrations were assumed to remain stable, even though minor fluctuations may occur in real-world applications. Since H_2S is typically the dominant contaminant, this approach ensures a conservative and robust system design that remains effective across different operational conditions.

One of the key computational trade-offs in this study concerns the 100-kW system, where a larger spatial step size (0.01 m vs. 0.001 m in the 3-kW case) was necessary to maintain feasible simulation times. While this approach ensures the model remains computationally manageable, it introduces a lower resolution of the adsorption front movement, resulting in small numerical uncertainties in breakthrough time estimation, particularly at lower H_2S concentrations, where adsorption front propagation is more gradual. Despite these minor deviations, the model remains a valuable predictive tool for biogas purification design. Future improvements, such as adaptive meshing techniques or refined numerical solvers, could further enhance accuracy while keeping computational costs under control.

Although the adsorption model developed in this study has been validated against lab-scale experimental data, further validation with full-scale SOFC-integrated biogas purification systems remains a key step for future research. Comparisons with existing biogas cleaning studies are limited, as most real-world applications focus on ICEs, which tolerate H_2S concentrations up to 150 ppm (Gandiglio et al., 2016) and do not require deep desulfurization comparable to the <1 ppm threshold needed for SOFCs (Wang et al., 2014). Additionally, validation requires precise knowledge of the reactor configuration, sorbent properties, and operational conditions, which are not always available in literature studies. Future work should focus on obtaining long-term operational data from real SOFC installations, allowing for a more comprehensive assessment of model performance under industrial conditions.

4. Conclusions

This study presents a comprehensive techno-economic assessment of biogas cleaning systems and their impact on the levelized cost of electricity (LCOE) for small to medium biogas-fueled SOFC systems, specifically at 3-kW and 100-kW scales. A central contribution of this work is the development of a mathematical adsorption model that enables precise prediction of transient contaminant concentration profiles,

facilitating the design and scalability of cleaning units for larger applications. This model adapts dynamically to initial conditions - such as feed concentration, contaminant types, flow rates, sorbent material, and reactor volume - and has been rigorously validated against experimental data to ensure its reliability for real-world SOFC applications.

In addition to the model, two configurations for managing H_2S contamination were analyzed: a single-vessel setup and an innovative lead-and-lag setup. The lead-and-lag configuration leverages a two-reactor series to extend sorbent usage and minimize operational interruptions, an advantage especially pronounced in the proposed equivalent cumulative concentration approach, which optimizes sorbent behavior modeling and computational efficiency.

The results of this study underscore the significant potential of SOFCs powered by biogas as an efficient and sustainable solution for renewable energy generation. The development of a flexible and cost-effective biogas clean-up unit for the deep removal of critical sulfur-based impurities can significantly improve the biogas utilization in high-efficiency fuel cell systems. The developed adsorption model accurately predicts contaminant concentration profiles, supporting the design of scalable cleaning units.

The comprehensive techno-economic analysis demonstrates that:

- In 3-kW systems, capital and operational expenditures for SOFC unit predominantly drive costs, contributing 56–70 % of the levelized cost of electricity. The biogas cleaning system significantly impacts the LCOE, constituting 30–37 % in single-vessel configurations and 35–44 % in lead-and-lag configurations, with the largest portion attributed to sorbent mass replacement costs.
- In 100-kW systems, investment costs for the SOFC decrease due to economies of scale, while the biogas cleaning system impact becomes more pronounced. Despite higher initial costs, the lead-and-lag configuration effectively reduces operational costs by minimizing sorbent material consumption and enhancing unit availability, enabling sorbent replacement without disrupting plant operations. This leads to a slightly lower LCOE compared to the single-vessel configuration.
- For larger-scale plants, the single-vessel configuration proves to be cost-effective. In contrast, the lead-and-lag configuration is more suitable for smaller-scale plants, thanks to its operational advantages and lower long-term costs. Overall, the analysis shows that the LCOE remains competitive with small-scale electric generation plants, with values below 0.32 €/kWh for 3-kW systems and below 0.12 €/kWh for 100-kW plants.
- The sensitivity analysis for the 100-kW plant demonstrates that the variations in sorbent costs, ranging from 2 €/kg to 20 €/kg, show a direct correlation with LCOE, with higher sorbent costs leading to an increase in LCOE across all H_2S concentrations. Notably, the lead-and-lag configuration exhibits greater economic advantages at elevated sorbent costs due to improved sorbent utilization and reduced replacement frequency.
- Similarly, the sensitivity analysis of sorbent mass indicates that lower sorbent masses result in higher LCOE due to increased replacement frequency, which incur not only material costs, but also operational expenses related to labor and disposal. Conversely, higher sorbent masses stabilize LCOE across configurations, with the lead-and-lag setup consistently demonstrating cost advantages.

CRediT authorship contribution statement

Elena Rozzi: Writing – original draft, Visualization, Validation, Software, Methodology, Investigation. **Marta Gandiglio:** Writing – review & editing, Supervision, Methodology, Investigation, Conceptualization. **Andrea Lanzini:** Writing – review & editing, Supervision. **Massimo Santarelli:** Writing – review & editing, Supervision.

Declaration of competing interest

The authors declare that they have no known competing financial interests or personal relationships that could have appeared to influence the work reported in this paper.

Acknowledgements

The study was conducted in the framework of the Waste2Watts EU project (https://cordis.europa.eu/project/id/826234). This project has received funding from the Fuel Cells and Hydrogen 2 Joint Undertaking under grant agreement No 826234. This Joint Undertaking receives support from the European Union's Horizon 2020 research and innovation programme, Hydrogen Europe and Hydrogen Europe research.

Appendix A. Supplementary data

Supplementary data to this article can be found online at https://doi.org/10.1016/j.jclepro.2025.145382.

Data availability

Data will be made available on request.

References

Awe, O.W., Minh, D.P., Lyczko, N., Nzihou, A., Zhao, Y., 2017. Laboratory-scale investigation of the removal of hydrogen sulfide from biogas and air using industrial waste-based sorbents. J. Environ. Chem. Eng. 5, 1809–1820. https://doi.org/10.1016/j.jece.2017.03.023.

Calbry-Muzyka, A., Madi, H., Rüsch-Pfund, F., Gandiglio, M., Biollaz, S., 2022. Biogas composition from agricultural sources and organic fraction of municipal solid waste. Renew. Energy 181, 1000–1007. https://doi.org/10.1016/j.renene.2021.09.100.

Calbry-Muzyka, A.S., Gantenbein, A., Schneebeli, J., Frei, A., Knorpp, A.J., Schildhauer, T.J., Biollaz, S.M.A., 2019. Deep removal of sulfur and trace organic compounds from biogas to protect a catalytic methanation reactor. Chem. Eng. J. 360, 577–590. https://doi.org/10.1016/j.cej.2018.12.012.

Chauveau, R., Grévillot, G., Marsteau, S., Vallières, C., 2013. Values of the mass transfer coefficient of the linear driving force model for VOC adsorption on activated carbons. Chem. Eng. Res. Des. 91, 955–962. https://doi.org/10.1016/j.cherd.2012.09.019.

Cherif, H., 2016. Study and modeling of separation methods H2S from methane, selection of a method favoring H2S valorization (phdthesis). Université Paris sciences et lettres. URL: https://pastel.hal.science/tel-01764942/file/2016PSLEM074_archivage.pdf.

Cigolotti, V., Genovese, M., 2021. Stationary Fuel Cell Applications: Current and Future Technologies - Costs, Performance, and Potential. IEA Technology Collaboration. URL: https://www.ieafuelcell.com/fileadmin/publications/2021/2021_AFCTCP_Stationary_Application_Performance.pdf.

Comsos, 2020. Comsos - commercial-scale SOFC systems [WWW Document]. URL. https://www.comsos.eu/. (Accessed 10 November 2024).

Coppola, G., Papurello, D., 2019. Biogas cleaning: activated carbon regeneration for H2S removal. Cleanroom Technol. 1, 40–57. https://doi.org/10.3390/cleantechnol1010004.

Costa, C., Cornacchia, M., Pagliero, M., Fabiano, B., Vocciante, M., Reverberi, A.P., 2020. Hydrogen sulfide adsorption by iron oxides and their polymer composites: a case-study application to biogas purification. Materials 13, 4725. https://doi.org/10.3390/ma13214725.

da Silva, M.T.Q.S., do Rocio Cardoso, M., Veronese, C.M.P., Mazer, W., 2022. Tortuosity: a brief review. Mater. Today: Proceedings, 3rd International Congress on Materials & Structural Stability 58, 1344–1349. https://doi.org/10.1016/j.matpr.2022.02.228.

Demosofc, 2020. DEMOSOFC FCH2-JU project. Url: http://www.demosofc.eu/. (Accessed 11 July 2024).

Duma, Z., Makgwane, P.R., Masukume, M., Swartbooi, A., Rambau, K., Mehlo, T., Mavhungu, T., 2024. A comprehensive review of metal-organic frameworks sorbents and their mixed-matrix membranes composites for biogas cleaning and CO2/CH4 separation. Materials Today Sustainability 27, 100812. https://doi.org/10.1016/j.mtsust.2024.100812.

European Biogas Association, 2022. Statistical Report - Tracking biogas and biomethane deployment across Europe, Brussels. https://www.europeanbiogas.eu/_trashed-3/.

Farooq, S., Ruthven, D.M., 1990. Heat effects in adsorption column dynamics. 2. In: Experimental Validation of the One-Dimensional Model, vol. 29. ACS Publications. https://doi.org/10.1021/ie00102a020.

Gandiglio, M., Drago, D., Santarelli, M., 2016. Techno-economic analysis of a solid oxide fuel cell installation in a biogas plant fed by agricultural residues and comparison with alternative biogas exploitation paths. Energy Procedia, ATI 2016 - 71st Conference of the Italian Thermal Machines Engineering Association 101, 1002–1009. https://doi.org/10.1016/j.egypro.2016.11.127.

Gandiglio, M., Marocco, P., Nieminen, A., Santarelli, M., Kiviaho, J., 2024. Energy and environmental performance from field operation of commercial-scale SOFC systems. Int. J. Hydrogen Energy 85, 997–1009. https://doi.org/10.1016/j.ijhydene.2024.08.332.

Gandiglio, M., Saberi Mehr, A., MosayebNezhad, M., Lanzini, A., Santarelli, M., 2020a. Solutions for improving the energy efficiency in wastewater treatment plants based on solid oxide fuel cell technology. J. Clean. Prod. 247, 119080. https://doi.org/10.1016/j.jclepro.2019.119080.

Gandiglio, M., Lanzini, A., Santarelli, M., Acri, M., Hakala, T., Rautanen, M., 2020b. Results from an industrial size biogas-fed SOFC plant (the DEMOSOFC project). International Journal of Hydrogen Energy, 22nd World Hydrogen Energy Conference 45, 5449–5464. https://doi.org/10.1016/j.ijhydene.2019.08.022.

Gandiglio, M., 2022. Design and operation of an industrial size adsorption-based cleaning system for biogas use in fuel cells. Energy 259, 124941. https://doi.org/10.1016/j.energy.2022.124941.

Giarola, S., Forte, O., Lanzini, A., Gandiglio, M., Santarelli, M., Hawkes, A., 2018. Techno-economic assessment of biogas-fed solid oxide fuel cell combined heat and power system at industrial scale. Appl. Energy 211, 689–704. https://doi.org/10.1016/j.apenergy.2017.11.029.

IEA, 2020. Levelised Cost of Electricity Calculator – Data Tools, IEA. https://www.iea.org/data-and-statistics/data-tools/levelised-cost-of-electricity-calculator (accessed October 25, 2024).

Lanzini, A., Madi, H., Chiodo, V., Papurello, D., Maisano, S., Santarelli, M., Van herle, J., 2017. Dealing with fuel contaminants in biogas-fed solid oxide fuel cell (SOFC) and molten carbonate fuel cell (MCFC) plants: degradation of catalytic and electro-catalytic active surfaces and related gas purification methods. Prog. Energy Combust. Sci. 61, 150–188. https://doi.org/10.1016/j.pecs.2017.04.002.

Li, S., Deng, S., Zhao, L., Zhao, R., Lin, M., Du, Y., Lian, Y., 2018. Mathematical modeling and numerical investigation of carbon capture by adsorption: literature review and case study. Appl. Energy 221, 437–449. https://doi.org/10.1016/j.apenergy.2018.03.093.

Lopes, F.V.S., Grande, C.A., Rodrigues, A.E., 2011. Activated carbon for hydrogen purification by pressure swing adsorption: multicomponent breakthrough curves and PSA performance. Chem. Eng. Sci. 66, 303–317. https://doi.org/10.1016/j.ces.2010.10.034.

Ma, C., Yu, H., Monticone, G., Ma, S., Van herle, J., Wang, L., 2024. Techno-economic evaluation of biogas-fed SOFC systems with novel biogas purification and carbon capture technologies. Renew. Energy 235, 121302. https://doi.org/10.1016/j.renene.2024.121302.

Micoli, L., Bagnasco, G., Turco, M., 2014. H2S removal from biogas for fuelling MCFCs: new adsorbing materials. Int. J. Hydrogen Energy 39, 1783–1787. https://doi.org/10.1016/j.ijhydene.2013.10.126.

Molino, G., Gandiglio, M., Fiorilli, S., Lanzini, A., Drago, D., Papurello, D., 2022. Design and performance of an adsorption bed with activated carbons for biogas purification. Molecules 27, 7882. https://doi.org/10.3390/molecules27227882.

MosayebNezhad, M., Mehr, A.S., Gandiglio, M., Lanzini, A., Santarelli, M., 2018. Techno-economic assessment of biogas-fed CHP hybrid systems in a real wastewater treatment plant. Appl. Therm. Eng. 129, 1263–1280. https://doi.org/10.1016/j.applthermaleng.2017.10.115.

Oluleye, G., Hawkes, A., 2020. DEMOnstration of Large SOFC System Fed with Biogas from WWTP: SOFC-Based CHP Market Potential Analysis- No Deliverable 6.1. URL: http://www.demosofc.eu/wp-content/uploads/2017/10/SOFC-based-CHP-market-potential-analysis.pdf.

Paglini, R., Gandiglio, M., Lanzini, A., 2022. Technologies for deep biogas purification and use in zero-emission fuel cells systems. Energies 15, 3551. https://doi.org/10.3390/en15103551.

Papadias, D.D., Ahmed, S., Kumar, R., 2012. Fuel quality issues with biogas energy – an economic analysis for a stationary fuel cell system. Energy, Integration and Energy System Engineering, European Symposium on Computer-Aided Process Engineering 44, 257–277. https://doi.org/10.1016/j.energy.2012.06.031.

Papurello, D., Schuhfried, E., Lanzini, A., Romano, A., Cappellin, L., Märk, T.D., Silvestri, S., Biasioli, F., 2014. Influence of co-vapors on biogas filtration for fuel cells monitored with PTR-MS (Proton Transfer Reaction-Mass Spectrometry). Fuel Process. Technol. 118, 133–140. https://doi.org/10.1016/j.fuproc.2013.08.011.

Papurello, D., Schuhfried, E., Lanzini, A., Romano, A., Cappellin, L., Märk, T.D., Silvestri, S., Santarelli, M., Biasioli, F., 2015a. Proton transfer reaction-mass spectrometry as a rapid inline tool for filter efficiency of activated charcoal in support of the development of Solid Oxide Fuel Cells fueled with biogas. Fuel Process. Technol. 130, 78–86. https://doi.org/10.1016/j.fuproc.2014.09.042.

Papurello, D., Tognana, L., Lanzini, A., Smeacetto, F., Santarelli, M., Belcari, I., Silvestri, S., Biasioli, F., 2015b. Proton transfer reaction mass spectrometry technique for the monitoring of volatile sulfur compounds in a fuel cell quality clean-up system. Fuel Process. Technol. 130, 136–146. https://doi.org/10.1016/j.fuproc.2014.09.041.

Papurello, D., Tomasi, L., Silvestri, S., Santarelli, M., 2016. Evaluation of the Wheeler-Jonas parameters for biogas trace compounds removal with activated carbons. Fuel Process. Technol. 152, 93–101. https://doi.org/10.1016/j.fuproc.2016.06.006.

Papurello, D., Santarelli, M., Fiorilli, S., 2018. Physical activation of waste-derived materials for biogas cleaning. Energies 11, 2338. https://doi.org/10.3390/en11092338.

Papurello, D., Gandiglio, M., Kafashan, J., Lanzini, A., 2019a. Biogas purification: a comparison of adsorption performance in D4 siloxane removal between commercial activated carbons and waste wood-derived char using isotherm equations. Processes 7, 774. https://doi.org/10.3390/pr7100774.

Papurello, D., Gandiglio, M., Lanzini, A., 2019b. Experimental analysis and model validation on the performance of impregnated activated carbons for the removal of hydrogen sulfide (H2S) from sewage biogas. Processes 7, 548. https://doi.org/10.3390/pr7090548.

Papurello, D., Silvestri, S., Lanzini, A., 2019c. Biogas cleaning: trace compounds removal with model validation. Separ. Purif. Technol. 210, 80–92. https://doi.org/10.1016/j.seppur.2018.07.081.

Papurello, D., Lanzini, A., Bressan, M., Santarelli, M., 2020. H2S removal with sorbent obtained from sewage sludges. Processes 8, 130. https://doi.org/10.3390/pr8020130.

Patton, A., Crittenden, B.D., Perera, S.P., 2004. Use of the linear driving force approximation to guide the design of monolithic adsorbents. Chem. Eng. Res. Des. 82, 999–1009. https://doi.org/10.1205/0263876041580749.

Pera, L., Gandiglio, M., Marocco, P., Pumiglia, D., Santarelli, M., 2024. Trace contaminants in biogas: biomass sources, variability and implications for technology applications. J. Environ. Chem. Eng. 12, 114478. https://doi.org/10.1016/j.jece.2024.114478.

Ratnakar, R.R., Dindoruk, B., 2022. The role of diffusivity in oil and gas industries: fundamentals, measurement, and correlative techniques. Processes 10, 1194. https://doi.org/10.3390/pr10061194.

Rozzi, E., Minuto, F.D., Lanzini, A., 2024. Techno-economic dataset for hydrogen storage-based microgrids. Data Brief 56, 110795. https://doi.org/10.1016/j.dib.2024.110795.

Samanta, S., Roy, D., Roy, S., Smallbone, A., Roskilly, A.P., 2023. Techno-economic analysis of a fuel-cell driven integrated energy hub for decarbonising transportation. Renew. Sustain. Energy Rev. 179, 113278. https://doi.org/10.1016/j.rser.2023.113278.

Santoni, F., Gislon, P., Rozzi, E., Gandiglio, M., McPhail, S., Lanzini, A., Pagani, M., Fiorilli, S., 2024. Hydrogen sulphide and carbonyl sulphide removal from biogas for exploitation in high-temperature fuel cells. Waste Biomass Valor 15, 577–597. https://doi.org/10.1007/s12649-023-02212-6.

Turton, R., Bailie, R.C., Whiting, W.B., Shaeiwitz, J.A., Bhattacharyya, D., 2012. Cost equations and curves for the CAPCOST program. In: Analysis, Synthesis and Design of Chemical Processes. Prentice-Hall, pp. 923–954. URL: https://richardturton.faculty.wvu.edu/publications/analysis-synthesis-and-design-of-chemical-processes-5th-edition.

W2W, 2022. Unlocking unused bio-WASTE resources with loW cost cleAning and Thermal inTegration with Solid oxide fuel cells | WASTE2WATTS Project | Fact Sheet | H2020 [WWW Document]. CORDIS | European Commission. URL. https://cordis.europa.eu/project/id/826234. (Accessed 28 October 2024).

Wakao, N., Funazkri, T., 1978. Effect of fluid dispersion coefficients on particle-to-fluid mass transfer coefficients in packed beds: correlation of sherwood numbers. Chem. Eng. Sci. 33, 1375–1384. https://doi.org/10.1016/0009-2509(78)85120-3.

Wang, F., Wang, W., Qu, J., Zhong, Y., Tade, M.O., Shao, Z., 2014. Enhanced sulfur tolerance of nickel-based anodes for oxygen-ion conducting solid oxide fuel cells by incorporating a secondary water storing phase. Environ. Sci. Technol. 48, 12427–12434. https://doi.org/10.1021/es503603w.

Wasajja, H., Lindeboom, R.E.F., van Lier, J.B., Aravind, P.V., 2020. Techno-economic review of biogas cleaning technologies for small scale off-grid solid oxide fuel cell applications. Fuel Process. Technol. 197, 106215. https://doi.org/10.1016/j.fuproc.2019.106215.

Yoon, Y.H., Nelson, J.H., 1984. Application of gas adsorption kinetics I. A theoretical model for respirator cartridge service life. Am. Ind. Hyg. Assoc. J. 45, 509–516. https://doi.org/10.1080/15298668491400197.

Zulkefli, N.N., Masdar, M.S., Isahak, W.R.W., Jahim, J., Majlan, E.H., Rejab, S.A.M., Lye, C.C., 2017. Mathematical modelling and simulation on the adsorption of Hydrogen Sulfide (H2S) gas. IOP Conf. Ser. Mater. Sci. Eng. 206, 012069. https://doi.org/10.1088/1757-899X/206/1/012069.